Exchange effects in spin-polarized transport through carbon nanotube quantum dots

Christoph Schenke, Sonja Koller, Leonhard Mayrhofer, and Milena Grifoni
Institut für Theoretische Physik, Universität Regensburg, 93035 Regensburg, Germany
(Received 20 March 2009; revised manuscript received 9 June 2009; published 10 July 2009)

We investigate linear and nonlinear transport across single-walled carbon nanotube quantum dots weakly coupled to spin-polarized leads. We consider metallic tubes of finite length and small diameter, where not only forward-scattering contributions of the Coulomb potential, but also short-ranged processes play an important role. In particular, they induce exchange effects leading for electron fillings $4n+2$ either to a nondegenerate ground state of spin $S=0$ or to a triplet ground state. In the linear regime we present analytical results for the conductance—for both the $S=0$ and the triplet ground state—and demonstrate that an external magnetic field is crucial to reveal the spin nature of the ground states. In the nonlinear regime we show stability diagrams that clearly distinguish between the different ground states. We observe a negative differential conductance (NDC) effect in the $S=0$ ground state for antiparallel lead magnetization. In presence of an external magnetic field, spin blockade effects can be detected, again leading to NDC effects for both ground states.

DOI: 10.1103/PhysRevB.80.035412 PACS number(s): 73.63.Fg, 72.25.−b, 73.23.Hk, 85.75.−d

I. INTRODUCTION

Since their discovery by Iijima and Ichihashi[1] in 1993, single-walled carbon nanotubes (SWNTs) have attracted attention due to their remarkable electronic and mechanical properties.[2,3] At low energies, they represent an almost perfect realization of a one-dimensional (1D) system of interacting electrons with an additional orbital degree of freedom due to the sublattice structure of graphene. Accounting for spin and orbital degrees of freedom implies that for nanotubes a shell structure is expected, where each shell can accommodate up to four electrons. In the absence of Coulomb interaction the energy levels are spin degenerate, while the orbital degeneracy is usually lifted due to the nanotube finite length. Coulomb interactions, however, modify this picture. The sublattice structure of graphene gives rise to a distinction between electron interactions on the same and on different sublattices. Therefore, besides the long-ranged forward-scattering processes, also short-ranged interaction processes play a role in small-diameter tubes.[4–7] These short-ranged interactions cause in finite-size nanotubes exchange effects leading for a tube filling of $4n+2$ to a ground state with either total spin $S=0$ or $S=\hbar$ (a triplet).[7] Signatures of the exchange interactions have indeed been inferred from stability diagrams of carbon-nanotube-based quantum dots.[8–10] In particular it was shown by Moriyama *et al.*[8] that an applied magnetic field can be used to reversibly change the ground state from the singlet to one of the triplet states.

Recently, carbon nanotubes have also attracted much attention for their potential applications in spintronic devices.[11] They are particularly interesting because they have a long spin lifetime and can be contacted with ferromagnetic materials. Indeed, spin-dependent transport in carbon nanotube spin valves has been demonstrated by various experimental groups,[12–14] ranging from the Fabry-Pérot[12,13] to the Kondo regime.[14]

From the theoretical point of view, spin-dependent transport in interacting SWNTs has been discussed so far in the limit of very long nanotubes,[15] for tubes in the Fabry-Pérot regime[16] and for SWNT-based quantum dots.[17–19] In the three latter works the characteristic four-electron shell filling could be observed in the stability diagrams. In Ref. 17 however, focus was on medium-to-large diameter SWNTs where exchange effects can be neglected. The studies in Refs. 18 and 19 are based on the theory by Oreg *et al.*,[6] where exchange interactions are treated on a mean-field level, and focus predominantly on shot noise[18] and cotunnelling[19] effects.

In this work we generalize the previous investigations of Ref. 17 to include the short-range Coulomb interactions causing exchange splittings of the six otherwise degenerate (at vanishing orbital mismatch) $4n+2$ filling ground states. The leads are either parallel or antiparallel spin-polarized and weakly coupled to the SWNT, see Fig. 1. In the low bias regime we derive analytical formulas for the conductance for both large and small orbital mismatch corresponding to an $S=0$ and $S=\hbar$ ground state, respectively, at $4n+2$ filling. In the high bias regime we numerically calculate the stability diagrams for the two possible ground states. We show several differences in transport between parallel and antiparallel lead magnetization, as e.g., a negative differential conductance (NDC) effect occurring only for the $S=0$ ground state and antiparallel magnetization. We further include in the calculations a parallel magnetic field leading to a Zeeman splitting for all states with total spin unequal to zero. It is then possible to observe spin blocking effects due to transport channels that trap the system in the triplet state with $S_z=-\hbar$. Performing a magnetic field sweep, a ground

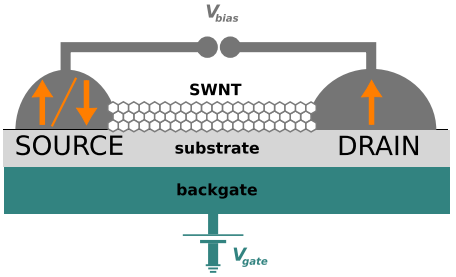

FIG. 1. (Color online) Single-electron-tunneling setup of a single-walled carbon nanotube (SWNT) which is weakly coupled to source and drain contacts. The contact magnetization may either be parallel or antiparallel as indicated by the arrows. The gate electrode allows to shift the chemical potential inside the SWNT.

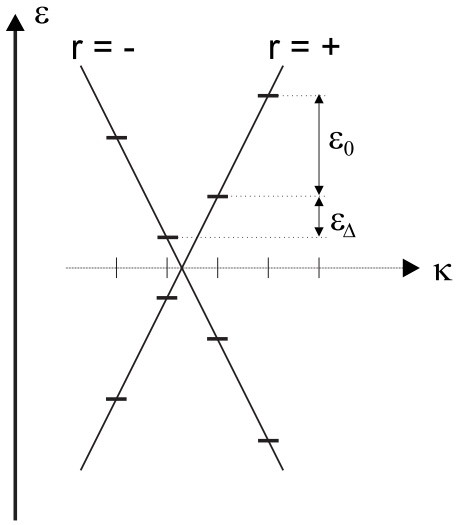

FIG. 2. The dispersion relation of a noninteracting SWNT with open boundary conditions. It is characterized by two linear branches, $r=\pm$, of slope $\pm\hbar v_F$ determined by the Fermi velocity v_F. The quantities ϵ_0 and ϵ_Δ are the intraband level spacing and the orbital mismatch energy, respectively.

state change may be obtained as it has been shown experimentally.[8]

The paper is organized as follows. In Sec. II we discuss the relevant features of the low energy Hamiltonian of interacting SWNTs with special focus on the filling $4n+2$. In Sec. III we describe the setup and method used to study spin-dependent transport in the sequential tunneling regime. Finally, in Sec. IV, we present our results for the conductance, while in Sec. V we focus on the nonlinear (finite bias) regime.

II. INTERACTING LOW ENERGY SPECTRUM

A. Interacting Hamiltonian

The starting point for a microscopic, but still analytical, treatment of SWNTs is a tight-binding ansatz for the wave function of the $2p_z$ electrons on the graphene honeycomb lattice. Including nearest-neighbor hopping matrix elements it yields an electron-hole symmetric band structure with a fully occupied valence band and an empty conduction band. Since the two bands touch at the corner points of the first Brillouin zone, the Fermi points, graphene is a zero gap semiconductor. Wrapping the considered sheet of graphene, i.e., imposing periodic boundary conditions (PBCs) around the circumference, yields a SWNT and leads to the formation of transverse subbands. For the low energy electronic structure of metallic SWNTs, only the subbands touching at the Fermi points are of relevance. In the following we consider armchair SWNTs of finite length and impose open boundary conditions (OBCs) at the two ends of the tube, i.e., that the wave function vanishes at the armchair edges. This condition mixes the two inequivalent Fermi points $F=\pm K_0$ from the underlying graphene first Brillouin zone and yields the linear dispersion relation of the finite-size SWNT shown in Fig. 2. It is characterized by two linear branches $r=\pm$ of slope $\pm\hbar v_F$ with the Fermi velocity $v_F \approx 8.1\cdot 10^5 \frac{m}{s}$. The allowed quasimomentum values are given by $\kappa=(n_\kappa+\Delta)\pi/L$, where $n_\kappa \in \mathbb{Z}$, L is the tube length, and Δ accounts for the fact that K_0 may not be an integer multiple of π/L. The kinetic part of the Hamiltonian, yielding the energy relative to the Fermi-sea, correspondingly reads

$$H_0 = \epsilon_0 \sum_{r\sigma} r \sum_{n_\kappa} n_\kappa c^\dagger_{r\sigma\kappa} c_{r\sigma\kappa} + \epsilon_\Delta \sum_{r\sigma} r N_{r\sigma}, \tag{1}$$

where $\epsilon_0=\hbar v_F \pi/L$ is the level spacing, and $\epsilon_\Delta \equiv \epsilon_0 \Delta$ is the band offset energy. Finally $c^\dagger_{r\sigma\kappa}$ creates an electron with momentum κ and spin σ in branch r and the operator $N_{r\sigma}$ counts the total electron number in branch r and of spin σ.

The interaction part of the Hamiltonian is given by

$$V = \frac{1}{2}\sum_{\sigma\sigma'} \int\int d^3r d^3r' \Psi^\dagger_\sigma(\vec{r}) \Psi^\dagger_{\sigma'}(\vec{r}') U(\vec{r}-\vec{r}') \Psi_{\sigma'}(\vec{r}') \Psi_\sigma(\vec{r}), \tag{2}$$

where Ψ, $\Psi^\dagger$ are fermion field operators and we use the Ohno potential,[20]

$$U(\vec{r}-\vec{r}') = U_0 \left[1 + \left(\frac{U_0 \epsilon |\vec{r}-\vec{r}'|}{14.397} \right)^2 \right]^{-1/2} \text{eV}, \tag{3}$$

with $U_0=15$ meV (Ref. 21) and $\epsilon \simeq 1.4-2.4$ (Ref. 4) is the dielectric constant of graphene. In the next step we express the three-dimensional (3D) electron operators in terms of the one-dimensional (1D) fermion-fields[22]

$$\psi_{rF\sigma}(x) = \frac{1}{\sqrt{2L}} \sum_\kappa e^{i\,\mathrm{sgn}(F)\kappa x} c_{r\sigma\kappa}, \tag{4}$$

and obtain

$$\Psi_\sigma(\vec{r}) = \sqrt{L} \sum_{rF} \mathrm{sgn}(F) \psi_{rF\sigma}(x) \sum_p f_{pr} \varphi_{pF}(\vec{r}). \tag{5}$$

Here $F=\pm K_0$ denotes the two independent Fermi points, $p=\pm$ the two sublattices of graphene, and the coefficients f_{pr} of the sublattice wave function $\varphi_{pF}(\vec{r})$ are given by $1/\sqrt{2}$ for $p=+$ and $-r/\sqrt{2}$ for $p=-$. The sublattice wave function itself reads

$$\varphi_{pF}(\vec{r}) = \frac{1}{\sqrt{N_L}} \sum_{\vec{R}\in L_G} e^{iFR_x} \chi_{p_z}(\vec{r}-\vec{R}-\vec{\tau}_p), \tag{6}$$

where N_L is the number of graphene lattice sites identified by the lattice vector $\vec{R}$, and L_G denotes the graphene honeycomb lattice in real space. Furthermore, $\chi_{p_z}(\vec{r}-\vec{R}-\vec{\tau}_p)$ is the p_z wave function of a carbon atom living on sublattice p, identified by the sublattice vector $\vec{\tau}_p$. Upon integrating Eq. (2) over the coordinates radial to the tube axis, one eventually arrives at a 1D interaction potential characterized by density-density and non-density-density contribution[7] so that the total Hamiltonian reads

$$H_\odot = H_0 + V_{\rho\rho} + V_{\mathrm{n}\rho\rho}. \tag{7}$$

With the help of bosonization[23] it is possible to diagonalize the density part $H_0+V_{\rho\rho}$. Eventually the bosonized and diagonalized Hamiltonian takes the form[7]

$$H_0 + V_{\rho\rho} = \sum_{j\delta q>0} \epsilon_{j\delta q} a^\dagger_{j\delta q} a_{j\delta q} + \frac{1}{2} E_c N_c^2 + \frac{1}{2} \sum_{r\sigma} N_{r\sigma} \left[-\frac{J}{2} N_{-r\sigma} + (\epsilon_0 - u^+) N_{r\sigma} + r\epsilon_\Delta \right]. \tag{8}$$

Besides the ground state, it accounts for all the possible fermionic and bosonic excitations of a SWNT. The bosonic excitations are described by the first term on the right-hand side. The indices refer to total/relative ($\delta = +/-$) charge/spin ($j = c/s$) modes. The energies $\epsilon_{j\delta q}$ are given by

$$\epsilon_{j\delta q} \cong \begin{cases} \epsilon_0 n_q \sqrt{1 + \dfrac{8W_q}{\epsilon_0}} & j\delta = c+, \\ \epsilon_0 n_q & j\delta = c-, s+, s-, \end{cases} \tag{9}$$

with $q = n_q \pi / L$ for $n_q \in \mathbb{Z}$ and

$$W_q = \frac{1}{(2L)^2} \int_0^L dx \int_0^L dx' U^{\text{long}}(x,x') 4 \cos(qx) \cos(qx'), \tag{10}$$

the contribution of the long-ranged density-density processes. Indeed $U^{\text{long}}(x,x') = [U^{\text{intra}} + U^{\text{inter}}]/2$ is the sum of the interaction potentials for electrons living in the same (intra) and different (inter) sublattices,

$$U^{\text{intra/inter}}(x,x') = \frac{L^2}{N_L^2} \sum_{\vec{R},\vec{R}'} \delta(x - R_x) \delta(x' - R'_x) \times U(\vec{R} - \vec{R}' + \vec{\tau}_p - \vec{\tau}_{\pm p}), \tag{11}$$

independent of the actual choice for p due to symmetry reasons. The second summand of Eq. (8) is the charging term with the charging energy $E_c = W_{q=0}$ and also comes from the long-range part of the Coulomb interaction. It counts the energy one has to spend to put $N_c = \Sigma_{r\sigma} N_{r\sigma}$ electrons on the dot, no matter what spin $\sigma \in \{\uparrow, \downarrow\}$ or pseudospin $r \in \{+,-\}$ they have. The second line of Eq. (8) starts with an exchange term favoring spin alignment. The exchange splitting,

$$J = \frac{1}{2N_L^2} \sum_{\vec{R},\vec{R}'} (1 + e^{-i2K_0(R_x - R'_x)}) \times [U(\vec{R} - \vec{R}') - U(\vec{R} - \vec{R}' + \vec{\tau}_p - \vec{\tau}_{-p})], \tag{12}$$

being proportional to the difference of the Coulomb interaction for electrons on the same and on different sublattices, accounts for the contribution of short-range processes. The next term in Eq. (8) reflects the energy cost for adding electrons of the same spin band in the same branch, i.e., the Pauli principle, where the correction u^+ is

$$u^+ = \frac{1}{4N_L^2} \sum_{\vec{R},\vec{R}'} e^{-i2K_0(R_x - R'_x)} \times [U(\vec{R} - \vec{R}') + U(\vec{R} - \vec{R}' + \vec{\tau}_p - \vec{\tau}_{-p})]. \tag{13}$$

Finally, the last term accounts for a possible band mismatch, see Fig. 2.

The eigenstates of $H_0 + V_{\rho\rho}$ are spanned by

$$|\vec{N}, \vec{m}\rangle = \prod_{j\delta q} \frac{(a^\dagger_{j\delta q})^{m_{j\delta q}}}{\sqrt{m_{j\delta q}!}} |\vec{N}, 0\rangle. \tag{14}$$

Here $\vec{N}$ and $\vec{m}$ denote the fermionic and the bosonic configuration, respectively, such that the state $|\vec{N}, 0\rangle$ has no bosonic excitation. The fermionic configuration is given by the number of electrons in each branch with a certain spin $\vec{N} = (N_{-\uparrow}, N_{-\downarrow}, N_{+\uparrow}, N_{+\downarrow})$. These eigenstates will be used to calculate the contribution of the nondensity part of the interaction, i.e., $\langle \vec{N}, \vec{m} | V_{\text{n}\rho\rho} | \vec{N}', \vec{m}' \rangle$. Away from half-filling, they only couple states close in energy and one is allowed to work with a truncated eigenbasis (we check convergence of the results as the basis is enlarged). As shown by Yoshioka and Odintsov,[24] for long SWNTs a Mott-insulating transition is expected to occur at half-filling due to umklapp scattering. As found in Ref. 7 umklapp processes acquire increasing weight as half-filling is approached also for finite-size tubes, a possible signature of the Mott instability, and the present theory breaks down. In recent experiments[25] the observation of the Mott transition in SWNT quantum dots was claimed.

B. Low energy spectrum away from half-filling

The low energy regime is where the energies that can be transferred to the system by the bias voltage and the temperature stay below ϵ_0. This means no bosonic excitations are present, i.e., $\vec{m} = (0,0,0,0)$, and also no fermionic excitations are allowed, i.e., the four bands will be filled as equal as possible: $|N_{r\sigma} - N_{r'\sigma'}| \leq 1 \, \forall \, r\sigma, r'\sigma'$. Our starting point are the eigenstates, Eq. (14), of the Hamiltonian in Eq. (8), which accounts for the kinetic and the density part of the full Hamiltonian. Now we have to split the examination into two cases.

At first we consider states with total charge N_c equal to $4n$, $4n+1$, and $4n+3$. Those are unambiguously described by the fermionic configuration $\vec{N}$ because they are not mixed by the exchange effects. The only impact of the short-range interaction terms on these states is given by an energy penalty for double occupation of one branch r, a common shift for all eigenstates with fixed $N_c \in \{4n, 4n+1, 4n+3\}$. Therefore we are left with[7]

$$E_{\vec{N}} = \frac{1}{2} E_c N_c^2 + u^+ \sum_r \min(N_{r\uparrow}, N_{r\downarrow}) + \frac{1}{2} \sum_{r\sigma} N_{r\sigma} \left[-\frac{J}{2} N_{-r\sigma} + (\epsilon_0 - u^+) N_{r\sigma} + r\epsilon_\Delta \right] \tag{15}$$

for the energy. If $\epsilon_\Delta \neq 0$, states with the maximum allowed number of electrons in the $r=-$ branch will be the ground states. For $N_c = 4n$ the pseudospin branches $r = \pm$ are equally occupied, yielding an unique $N_c = 4n$ ground state. The corresponding configuration is taken as reference configuration for the $N_c = 4n+1$, $4n+2$, and $4n+3$ cases. The lowest lying states for $N_c \in \{4n+1, 4n+3\}$ are presented in Fig. 3. E.g., for the case $N_c = 4n+1$ we obtain four possible states corresponding to

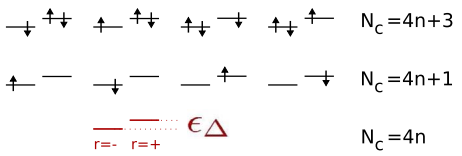

FIG. 3. (Color online) Lowest lying states for fillings $N_c=4n+1$ and $N_c=4n+3$. For simplicity only the configuration of the last partially filled shell is shown.

$\vec{N} \in \{(n+1,n,n,n),(n,n+1,n,n),(n,n,n+1,n),(n,n,n,n+1)\}$. For simplicity we introduce for the states with an unpaired electron in the $r=-$ branch the notation $|\uparrow,\cdot\rangle$, $|\downarrow,\cdot\rangle$. For electrons in the $r=+$ branch we set $|\cdot,\uparrow\rangle$, $|\cdot,\downarrow\rangle$.

Analogously, neglecting exchange effects and setting $\epsilon_\Delta=0$ for the moment, the ground states for the $N_c=4n+2$ filling are represented by the six states $|\uparrow,\uparrow\rangle$, $|\downarrow,\downarrow\rangle$, $|\uparrow,\downarrow\rangle$, $|\downarrow,\uparrow\rangle$, $|\uparrow\downarrow,\cdot\rangle$, and $|\cdot,\uparrow\downarrow\rangle$, where, e.g., $|\uparrow,\uparrow\rangle$ means two electrons with spin $\uparrow$ one on each branch $-$ and $+$. Here the different fermionic configurations mix under the influence of the $V_{n\rho\rho}$ processes and the ground-state structure will change dramatically due to off-diagonal contributions

$$\langle\uparrow,\downarrow|V_{n\rho\rho}|\downarrow,\uparrow\rangle = -J/2,$$

$$\langle\uparrow\downarrow,\cdot|V_{n\rho\rho}|\cdot,\uparrow\downarrow\rangle = J/2. \tag{16}$$

Diagonalization of the interaction matrix yields the ground-state spectrum as it is shown in Table I. The energies in the table are given relative to $E_{0,4n+2}=\frac{1}{2}E_cN_c^2+(2n^2+2n+1)(\epsilon_0-u^+)-\frac{J}{2}(2n^2+2n)+2u^+n$. It is clear that the states $|s\rangle$ and $|b\rangle$ will always be excited states, while the spin triplet, $S=\hbar$, is energy degenerate. Now the question arises which states, the triplet or the $|a\rangle$ state, are the ground state of the system. In accordance with Table I, the condition for a triplet ground state is given by

$$\epsilon_\Delta^2 < (u^+)^2 + Ju^+. \tag{17}$$

For a dielectric constant $\epsilon=1.4$ it holds $J=0.72$ Å$\frac{\epsilon_0}{d}$ and $u^+=0.22$ Å$\frac{\epsilon_0}{d}$. Hence we find in terms of the level spacing ϵ_0 and the tube diameter d,

TABLE I. The six lowest energy eigenstates for the filling $N_c=4n+2$ of an interacting SWNT. Due to short-ranged interactions there are three degenerate states of total spin $S=\hbar$ and three nondegenerate states of total spin $S=0$.

State	Relative energy	spin
$\|t_1\rangle=\|\uparrow,\uparrow\rangle$	$-J/2$	$\hbar$
$\|t_{-1}\rangle=\|\downarrow,\downarrow\rangle$	$-J/2$	$\hbar$
$\|t_0\rangle=\frac{1}{\sqrt{2}}(\|\uparrow,\downarrow\rangle+\|\downarrow,\uparrow\rangle)$	$-J/2$	$\hbar$
$\|s\rangle=\frac{1}{\sqrt{2}}(\|\uparrow,\downarrow\rangle-\|\downarrow,\uparrow\rangle)$	$+J/2$	0
$\|a\rangle=\frac{1}{\sqrt{c_1^2+1}}(-c_1\|\uparrow\downarrow,\cdot\rangle+\|\cdot,\uparrow\downarrow\rangle)$	$u^+-\sqrt{(\frac{J}{2})^2+\epsilon_\Delta^2}$	0
$\|b\rangle=\frac{1}{\sqrt{c_2^2+1}}(-c_2\|\uparrow\downarrow,\cdot\rangle+\|\cdot,\uparrow\downarrow\rangle)$	$u^++\sqrt{(\frac{J}{2})^2+\epsilon_\Delta^2}$	0
$c_1=\frac{2\epsilon_\Delta+\sqrt{J^2+(2\epsilon_\Delta)^2}}{J}$, $c_2=\frac{2\epsilon_\Delta-\sqrt{J^2+(2\epsilon_\Delta)^2}}{J}$		

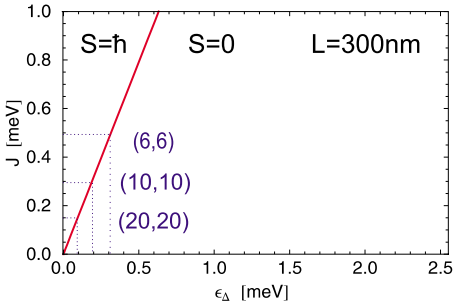

FIG. 4. (Color online) Phase diagram to determine the ground state of different tubes of length 300 nm. The chance to find a triplet ground state increases with increasing exchange parameter J, i.e., with decreasing tube diameters.

$$|\epsilon_\Delta| < 0.4548 \text{ Å}\frac{\epsilon_0}{d}. \tag{18}$$

Obviously this makes the triplet ground state more unlikely compared to the $S=0$ ground state as it can be seen in Fig. 4. For a (6,6) nanotube of 300 nm length, the band mismatch must be $\epsilon_\Delta < 0.3$ meV$\cong 0.06\epsilon_0$ to be in a triplet ground state. In the experiments Refs. 9 and 10 band mismatches are of the order of $0.3\epsilon_0$ and, as expected from our theory, $|a\rangle$ ground states are observed.

III. SPIN-DEPENDENT TRANSPORT

In this section we discuss the setup to evaluate spin-dependent transport across a SWNT weakly coupled to leads, see Fig. 1, and the main calculation tools. The Hamiltonian of the full system reads

$$H = H_\odot + \sum_{l=s,d} H_l + H_T + H_{ext}, \tag{19}$$

where $l=s,d$ denotes the Hamiltonian in the source and the drain contact, respectively. The leads magnetization is accounted for in terms of a Stoner Hamiltonian where the density of states, $\mathcal{D}_{l\sigma}(\epsilon)$, for the majority ($\sigma=\uparrow$) and the minority ($\sigma=\downarrow$) carriers are different. We treat the leads within the wide-band approximation, i.e., we regard the density of states as constant quantities to be evaluated at the leads chemical potentials μ_s and μ_d. We can thus define the polarization by ($l=s,d$),

$$P_l = \frac{\mathcal{D}_{l\uparrow}(\mu_l) - \mathcal{D}_{l\downarrow}(\mu_l)}{\mathcal{D}_{l\uparrow}(\mu_l) + \mathcal{D}_{l\downarrow}(\mu_l)}. \tag{20}$$

Moreover, we will consider a symmetric set up $\mathcal{D}_{s\sigma}=\mathcal{D}_{d\sigma}=\mathcal{D}_\sigma$ and $P_s=P_d=P$. The total density of states is given by $\mathcal{D}_{tot}=\mathcal{D}_\uparrow+\mathcal{D}_\downarrow$. We account for the bias voltage V_b in terms of the difference $eV_b=\mu_s-\mu_d$ between the electrochemical potentials in the source and drain leads. Further, H_T in Eq. (19) is the tunneling Hamiltonian which we will treat as a perturbation since weak coupling to the leads is assumed. Finally, H_{ext} describes the influence of the externally applied gate voltage V_g. The gate is capacitively coupled to the SWNT and hence contributes via a term $e\alpha V_gN_c$ with α a proportionality factor.

TABLE II. Parameter set of the 300 nm (6,6) nanotube investigated in this work.

Parameters	Label	Value
Length	L	300.06 nm
Diameter	d	0.81 nm
Dielectric constant	ϵ	1.4
⇓		
Charging energy	E_c	6.7 meV
Level spacing	ϵ_0	5.6 meV
Coulomb excess energy	u^+	0.15 meV
Exchange energy	J	0.49 meV
Orbital mismatch	ϵ_Δ	0 meV or 1.68 meV
Thermal energy	k_BT	4.0×10^{-3} meV
Transmission coefficient	$\mathcal{D}_{tot}\Phi$	1×10^{-4} meV

In order to evaluate the current-voltage characteristics we use the method developed in Ref. 17 where, starting from the Liouville equation for the density matrix of the full system, a generalized master equation (GME) for the reduced density matrix (RDM) ρ of the SWNT is obtained to second order in H_T. Once the stationary RDM is known, the stationary current through, e.g., the source lead is evaluated from the relation $I_s=eTr\{\rho\dot{N}_s\}$, where N_s is the number operator for electrons in the left lead. As this procedure with the relevant equations is thoroughly explained in Ref. 17, we refrain from repeating it here. The GME can be solved in analytic form in the linear regime, being the focus of the following Sec. IV. In the nonlinear regime, discussed in Sec. V, the differential conductance is evaluated numerically. Moreover, from here on we will focus on the transition between charge states $4n+1\leftrightarrow4n+2$, mirror symmetric to $4n+2\leftrightarrow4n+3$, as these two transitions are the ones that reveal exchange effects. The remaining transitions $4n\leftrightarrow4n+1$ and $4n+3\leftrightarrow4(n+1)$ will not qualitatively change due to the presence of short-range processes and we hence refer to the discussion in Ref. 17.

If not otherwise specified, we choose nanotubes described by the parameters in Table II: in order to obtain an $|a\rangle$ ground state we assume a band mismatch of $\epsilon_\Delta=0.3\epsilon_0=1.68$ meV, whereas for a triplet ground state we choose $\epsilon_\Delta=0$.

IV. LINEAR REGIME

A. Conductance at zero magnetic field

We focus on the conductance formulas for the two cases of tunneling from the $4n+1$ ground states into the $S=0$ ground state $|a\rangle$ or into the triplet ground states.

For the transition $|\sigma,\cdot\rangle\leftrightarrow|a\rangle$ the conductances in the case of parallel, G^P, and antiparallel, G^{AP}, magnetized leads are found to be

$$G_a^P=\frac{c^2e^2\pi}{\hbar}\frac{\gamma}{1+\gamma}\beta\mathcal{D}_{tot}\Phi\left|\frac{f(\mu_a)f(-\mu_a)}{2-f(\mu_a)}\right|, \tag{21a}$$

$$G_a^{AP}=\frac{(P^2-1)\gamma(1+\gamma)}{P^2(\gamma-1)^2-(\gamma+1)^2}G_a^P, \tag{21b}$$

with $c=\frac{c_1}{\sqrt{c_1^2+1}}$, the Fermi function $f(\mu)$ evaluated at the gate voltage dependent energy difference $\mu_a=E_{|a\rangle}-E_{|\sigma,\cdot\rangle}$ and β the inverse temperature. The parameters $\Phi=\Phi_s$ and $\gamma=\Phi_d/\Phi_s$ describe the possible asymmetric lead transparencies[17] (hereby, Φ is in second order of the tunneling coupling contained in H_T). The conductances are shown in Figs. 5(a) and 5(c) for the symmetric transparencies case $\gamma=1$ and $\mathcal{D}_{tot}\Phi=10^{-4}$ meV. Strikingly, in the parallel magnetized case there is *no* dependence on the polarization since there is never a blocking state involved in transport, see Fig. 5(b). For the antiparallel case, in contrast, transport is limited by the weakest channel (when there is a $\downarrow$ electron on the dot) and one can drive the conductance to zero by tuning the polarization to $P\to1$. This feature is explained in Fig. 5(d).

For the case of the triplet ground state we face a completely new situation. First, we have for $N_c=4n+1$ filling four degenerate states available because the band mismatch has been chosen to be zero. Second, we couple to three different states in the case of $N_c=4n+2$ rather than to just one. However, the conductance plots do not qualitatively change as it may be seen in Figs. 6(a) and 6(c). The conductance formulas read

$$G_{1,t}^P=\frac{3e^2\pi}{\hbar}\frac{\gamma}{1+\gamma}\beta\mathcal{D}_{tot}\Phi\left|\frac{f(\mu_t)f(-\mu_t)}{4-f(\mu_t)}\right|, \tag{22a}$$

$$G_{1,t}^{AP}=\frac{(P^2-1)\gamma(1+\gamma)}{P^2(\gamma-1)^2-(\gamma+1)^2}G_{1,t}^P. \tag{22b}$$

Compared to Eqs. (21a) and (21b) the prefactor changed from c^2 to 3 due to the three involved triplet states. The quantity $\mu_t=E_{|t\rangle}-E_1$ is the difference between the triplet and the $N_c=4n+1$ ground-state energies. In addition, the denominator in the term containing the Fermi functions has also changed to account for the degeneracy of the $4n+1$ filling states. The qualitative behavior, however, does not change compared to the case of an $|a\rangle$ ground state, such that one cannot determine the spin nature of the ground state from these plots alone.

B. Conductance in the presence of an external magnetic field

In this section we consider the influence of an externally applied magnetic field (Zeeman-field) which clearly reveals the character of the ground state for $4n+2$ and, moreover, may even change the ground state depending on the field strength. The field causes an additional Zeeman energy to states with a spin-component $S_z\neq0$. The sign is negative if the concerned state in the tube is parallel to the external field and positive if antiparallel. Thus, the chemical-potential differences appearing in Eqs. (21a), (21b), (22a), and (22b) will be shifted by $\pm E_z=\pm\mu_BB$. We use the convention $\mu_\uparrow=\mu-E_z$ and $\mu_\downarrow=\mu+E_z$. Furthermore, in order to improve the readability, we introduce the abbreviation $f_{\pm\uparrow/\downarrow}=f(\pm\mu_{\uparrow/\downarrow})$. The conductances for the antiparallel setup are

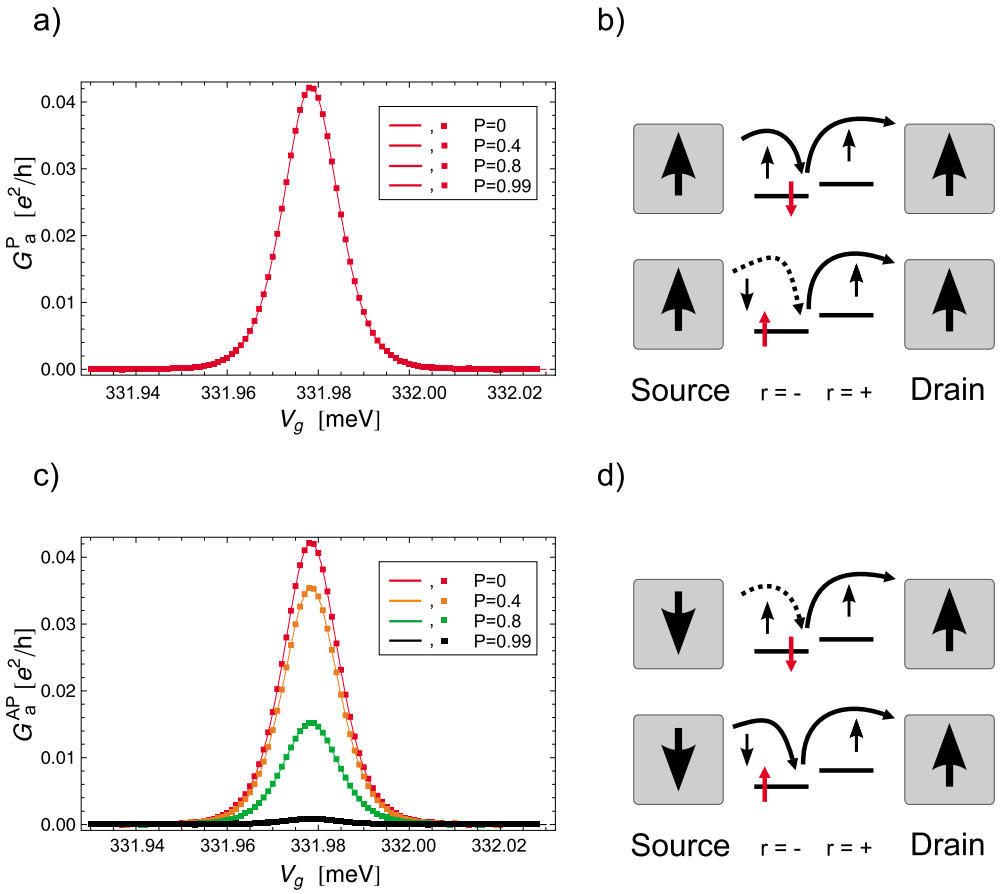

FIG. 5. (Color online) Panels (a) and (c): Conductance vs gate voltage for the $|\sigma,\cdot\rangle \leftrightarrow |a\rangle$ resonance for parallel, G_a^P, and antiparallel, G_a^{AP}, lead magnetization. In both cases the analytical predictions Eqs. (21a) and (21b) (continuous curves) perfectly match with the results from a numerical evaluation of the GME (squares). Strikingly G_a^P is independent of the leads polarization P, while G_a^{AP} is maximal at $P=0$. Panels (b) and (d): Schematic explanation of the different polarization dependence. The red spin specifies the spin of the state $|\sigma,\cdot\rangle$. The dashed/continuous arrows indicate rare/favorable tunneling processes. For parallel magnetization, panel (b), the fast tunneling channel is the one with an excess spin $\downarrow$ and the electron transferred from source to drain is always a majority electron $\uparrow$. If the initial dot spin is $\uparrow$, this is likely to tunnel to the drain, such that at the end of the tunneling process a spin flip has occurred, leaving the dot in the favorable configuration with a spin $\downarrow$. For antiparallel lead magnetization, panel (d), the fast channel corresponds to one electron in the dot with spin $\uparrow$. To this channel, however, is associated a spin flip. Because the situation with initial spin $\downarrow$ involves a rare tunneling process from the source lead, the conductance gets diminished by increasing polarization.

$$G_a^{AP}(E_z) = \frac{c^2 e^2 \pi}{2\hbar}\beta \mathcal{D}_{tot}\Phi \left| \frac{f_{+\uparrow}f_{+\downarrow}(1+P(\gamma+1)+\gamma)f_{-\downarrow}}{f_{+\downarrow}+f_{+\uparrow}f_{-\downarrow}} + \frac{f_{+\uparrow}f_{+\downarrow}(1-P(\gamma-1)+\gamma)f_{-\uparrow}}{f_{+\downarrow}+f_{+\uparrow}f_{-\downarrow}} \right| \tag{23a}$$

and

$$G_t^{AP}(E_z) = \frac{e^2\pi}{2\hbar}\beta \mathcal{D}_{tot}\Phi \times |\{f_{-\uparrow}f_{-\downarrow}\{[1+\gamma-P(1-\gamma)]f_{+\downarrow}(f_{-\downarrow}f_{+\uparrow}+2f_{+\downarrow}f_{-\uparrow}) + [1+\gamma+P(1-\gamma)]f_{+\uparrow}(f_{-\uparrow}f_{+\downarrow}+2f_{-\downarrow}f_{+\uparrow})\}\}/[f_{-\uparrow}(1 + f_{-\downarrow})(f_{-\downarrow}f_{+\uparrow}+f_{-\uparrow}f_{+\downarrow})+f_{-\downarrow}^2 f_{+\uparrow}^2]|. \tag{23b}$$

We do not find qualitative differences with respect to the zero magnetic field case: the conductances decrease in both cases with increasing polarization. In the following, we will therefore only focus on the parallel case, where we find interesting behavior for small Zemann splittings. The conductance formulas for parallel lead magnetization take the form

$$G_a^P(E_z) = \frac{c^2 e^2 \pi}{\hbar}\frac{\gamma}{1+\gamma}\beta \mathcal{D}_{tot}\Phi \times \left| \frac{f_{+\uparrow}f_{+\downarrow}[(P+1)f_{-\uparrow}-(P-1)f_{-\downarrow}]}{f_{+\uparrow}f_{+\downarrow}+f_{+\downarrow}f_{-\uparrow}+f_{+\uparrow}f_{-\downarrow}} \right| \tag{24a}$$

and

$$G_t^P(E_z) = \frac{e^2\pi}{2\hbar}\frac{\gamma}{1+\gamma}\beta \mathcal{D}_{tot}\Phi |\{f_{-\uparrow}f_{-\downarrow}[(P+1)f_{+\uparrow}(f_{-\uparrow}^2 f_{+\downarrow} + f_{+\uparrow}f_{-\uparrow}f_{+\downarrow}+2f_{+\uparrow}f_{-\uparrow}f_{-\downarrow}+2f_{+\uparrow}^2 f_{-\downarrow}) - (P-1)f_{+\downarrow}(f_{-\downarrow}^2 f_{+\uparrow}+2f_{+\downarrow}^2 f_{-\uparrow}+2f_{+\downarrow}f_{-\uparrow}f_{-\downarrow} + f_{+\downarrow}f_{+\uparrow}f_{-\downarrow})]\}/\{2f_{-\downarrow}^2 f_{+\uparrow}f_{-\uparrow}+f_{+\uparrow}^2 f_{-\uparrow}^2+f_{-\uparrow}^2 f_{+\downarrow}^2 + 2f_{-\uparrow}^2 f_{-\downarrow}f_{+\uparrow}+f_{-\downarrow}f_{-\uparrow}f_{+\uparrow}f_{+\downarrow}\}|. \tag{24b}$$

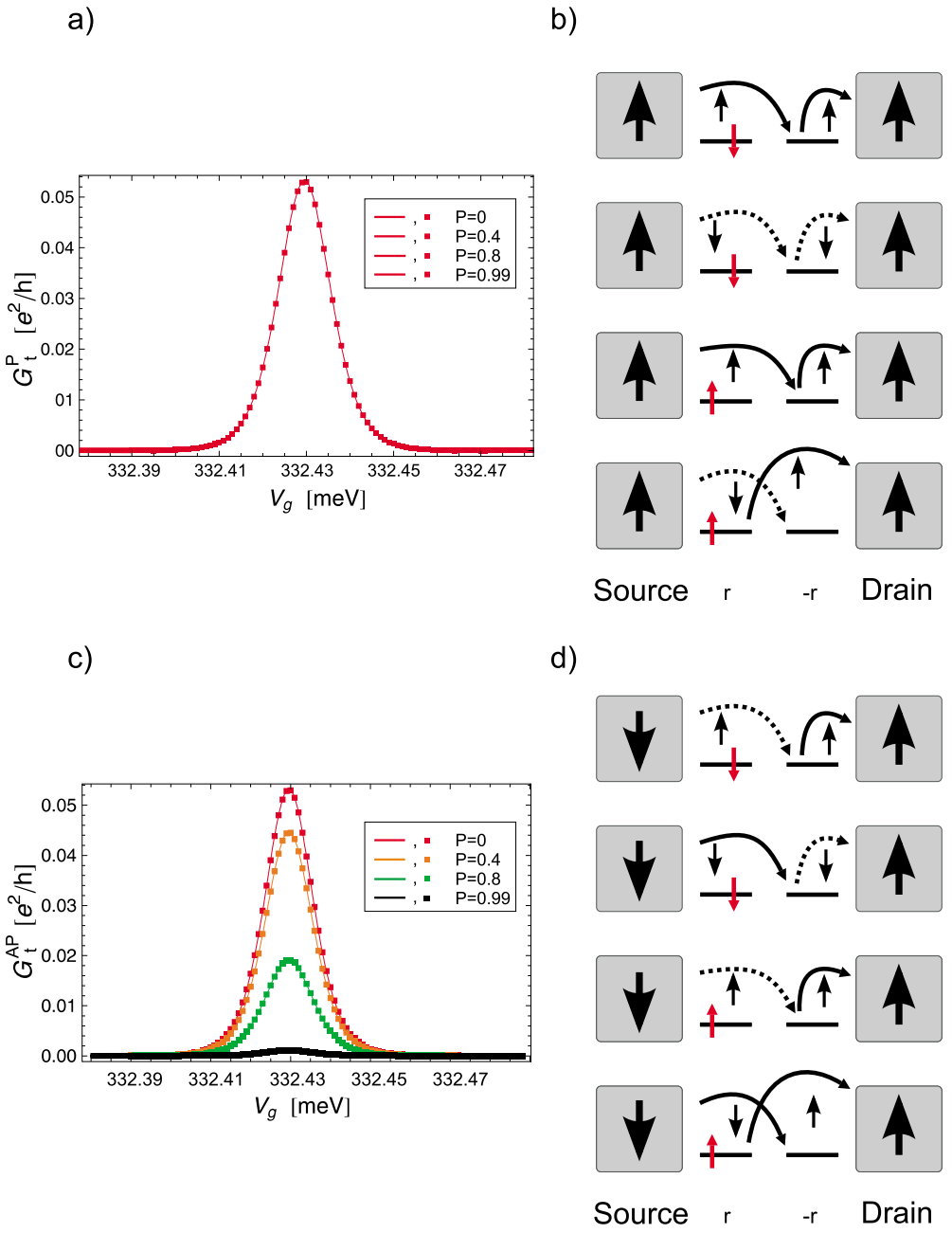

FIG. 6. (Color online) Panels (a) and (c): Conductance vs gate voltage at zero band mismatch (triplet ground state) for parallel, G_t^P, and antiparallel, G_t^{AP}, lead magnetization. G_t^P is independent of the leads polarization P, while G_t^{AP} is maximal at $P=0$. The absolute value of the conductance is slightly larger than for the $|\sigma,\cdot\rangle \leftrightarrow |a\rangle$ case since more channels are involved. Panels (b) and (d): Schematic explanation of the different polarization dependence. For simplicity we only drew the case in which the initial excess spin (red spin) is in the $r=+$ branch. For parallel magnetization, panel (b), the fast channel corresponds to the $|\uparrow,\cdot\rangle \leftrightarrow |t_{+1}\rangle$ transition which conserves the spin of the excess dot electron. For antiparallel magnetization, panel (d), the fast channel corresponds to an initial excess spin $\uparrow$ electron likely to tunnel to the drain and being replaced by a spin $\downarrow$ from the source. The situation with an initial spin $\downarrow$, however, corresponds to a weak channel. Increasing the polarization highly populates the $|t_{-1}\rangle$ state and transport decreases.

The corresponding plots can be seen in Figs. 7(a) and 8(a). In these calculations we considered a small magnetic field of 0.07 T which equals in magnitude the thermal energy of $k_BT=0.004$ meV. This provides a situation with a finite occupation probability for all included states. Specifically, this means that also states containing $\downarrow$ electrons will be populated, but the population of states containing $\uparrow$ electrons will be preferred. The first thing we observe in both Figs. 7(a) and 8(a) is that the once degenerate curves in Figs. 5(a) and 6(a) now split into distinct curves for the four different polarizations. Moreover, the peaks of the curves corresponding to less polarized leads continuously move to higher gate voltages. Finally the conductance *decreases/increases* with increasing polarization for the a/t cases, respectively. Let us examine the results starting with the $|a\rangle$ ground state. We will divide the analysis in two cases,

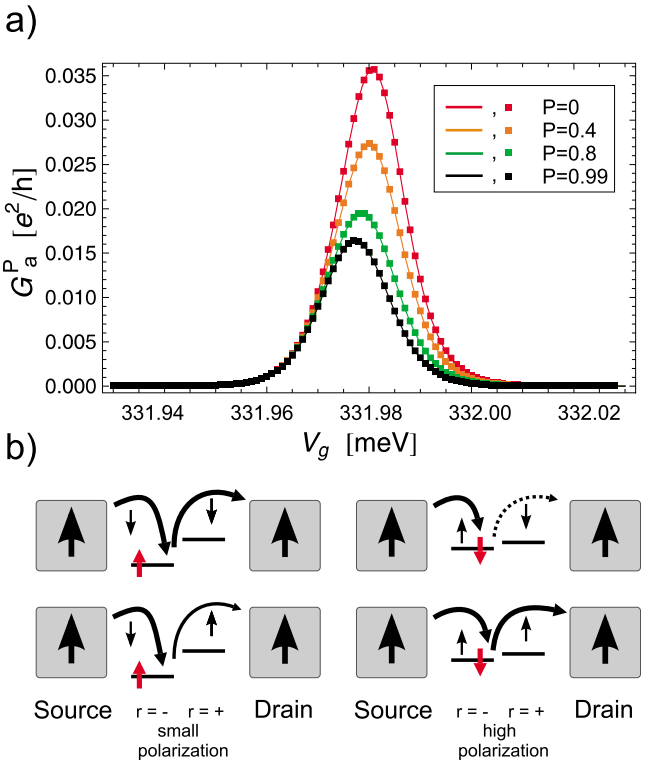

FIG. 7. (Color online) (a) Conductance near the $|\sigma,\cdot\rangle \leftrightarrow |a\rangle$ transition for parallel magnetized leads and applied magnetic field. The peaks corresponding to higher polarizations are shifted to lower gate voltages. (b) Schematic explanation of the polarization and gate-voltage dependence for small (left sketch) and large (right sketch) polarization. The red spin indicates the spin of the excess electron initially present on the dot. The thick and thin lines are frequent and less frequent transitions, while dashed lines indicate rare transitions. Large polarizations favor processes involving majority spins while, due to the extra required Zeeman energy, the Fermi function suppresses processes where a spin ↓ is transferred. Thus at small polarizations the transport is mostly mediated by spin ↓ electrons while at large polarizations ↑ electrons are preferred. Correspondingly the peak position is shifted to smaller gate voltages as the polarization is increased.

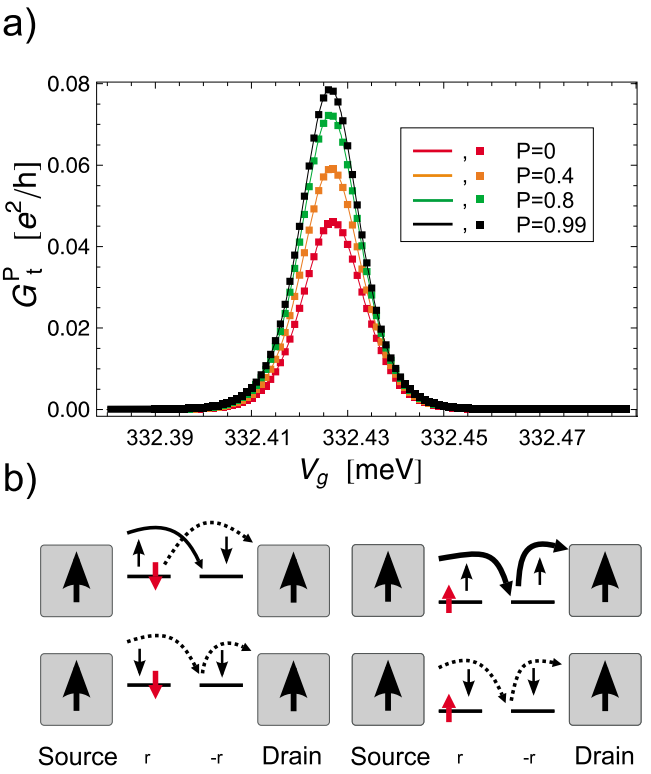

FIG. 8. (Color online) (a) Conductance near the triplet resonance for parallel magnetized leads and applied magnetic field. In contrast to the case of a singlet resonance, Fig. 7, transport increases as the polarization is enhanced. (b) Schematic explanation. At small leads polarization the distribution of ↑ electrons and ↓ electrons is almost equal. However, the $|t_1\rangle$ channel is preferred to the others. Increasing the polarization enhances the dominance of this channel and correspondingly the conductance. Simultaneously the conductance peak is shifted to lower gate voltage indicating the dominance of ↑ electrons.

slightly polarized leads and strongly polarized leads.

For only slightly polarized or nonpolarized leads the situation is intricate as we have to deal with *competing processes*. On the one hand there is a highly populated $|\uparrow,\cdot\rangle$ state and a slightly populated $|\downarrow,\cdot\rangle$ state in the tube. From this point of view, the system prefers ↓ electrons to tunnel into the $|a\rangle$ state and to leave the dot subsequently such that the tube always remains in the preferred $|\uparrow,\cdot\rangle$ state [Fig. 7, sketch (b), upper left panel]. Only rarely, the ↑ electron tunnels out, as this would result in a spin-flip to the disfavored $|\downarrow,\cdot\rangle$ state [Fig. 7, sketch (b), lower left panel]. On the other hand, entering of ↓ electrons is suppressed compared to transport of ↑ electrons, not so much by the small polarization, but mainly due to the Zeeman splitting in the involved Fermi functions: the chemical potential for ↓ electrons exceeds the one for ↑ electrons by $2E_z$ such that $f_{+\uparrow} > f_{+\downarrow}$ at any gate voltage. However, in the end it will be a mixture of mainly ↓ electrons and some ↑ electrons responsible for transport. This can also be seen by the fact that the curves for small polarizations are shifted to higher gate voltages which accounts for the higher chemical potential of the ↓ electrons. In addition, the total amplitude of the conductance is decreased compared to the case without the magnetic field, Fig. 5(a), as there is always a limiting element—either the small Fermi function or the small population—involved.

In the case of highly polarized leads we face the situation where there are very few ↓ electrons in the leads. As temperature provides a small, but nonzero population of the slightly excited state $|\downarrow,\cdot\rangle$, current mainly flows via the polarization favored ↑ electron channel. Since the chemical potential, the increment of the Fermi functions, is smaller than in the former case the transition takes place at slightly lower gate voltages. The situation again is visualized in the sketch (b) of Fig. 7, in the upper and lower right panel.

At the triplet resonance we observe not only quantitative, but also qualitative changes. The plot can be seen in Fig. 8(a) and all relevant tunneling processes are sketched in Fig. 8(b). Let us again start with unpolarized or just slightly polarized leads. Due to a large population of the spin ↑ states in the $N_c=4n+1$ case and of the $|t_1\rangle$ state in the $N_c=4n+2$ case transport is mainly mediated via the majority charge carriers, i.e., ↑ electrons [Fig. 8(b), upper right panel]. However, the

resulting current is smaller than in the case without magnetic field since it is harder to make use of the ↓ electrons that are still largely at disposal in the leads.

A high polarization decreases the number of ↓ electrons in the leads in favor of the ↑ electron number, and such transport via the already preferred $|t_1\rangle$ channel is strongly enhanced. As a consequence, the conductance by far *exceeds* the conductance without magnetic field and polarization. This effect should be detectable in an experimental setup and would give a possibility to distinguish between a triplet ground state and a $S=0$ ground state.

V. NONLINEAR REGIME

In the finite bias regime also excited states become available and, due to the resulting high number of involved states, it is necessary to calculate the current numerically. We show the current and the stability diagrams—the differential conductance $\frac{dI}{dV_b}(V_b, V_g)$ as a function of the gate and the bias voltage. The stability diagrams give a clear indication whether the involved ground state in the transition $4n+1 \leftrightarrow 4n+2$ is the $|a\rangle$ state or the triplet. In the case of antiparallel lead magnetization we find negative differential conductance (NDC) for transitions involving the $|a\rangle$ state. We also observe NDC for transitions involving the $|a\rangle$ state or the triplet if an external magnetic field is applied.

The current as a function of the gate and the bias voltage is shown in Fig. 9(a) for the $|a\rangle$ ground state and in Fig. 9(b) for the triplet ground state. All states with up to one bosonic excitation have been included in the calculation. A four-electron periodicity of the Coulomb diamonds is clearly seen. The change in color indicates a change in current and therefore the opening of a new channel. At high bias a smearing of the transitions due to the multitude of bosonic excitations is observed. In the remaining of this section we focus on the gate-voltage region relevant for the $4n+1 \leftrightarrow 4n+2$ transitions. In the plots of the differential conductance reported in the following we did not include the bosonic excitations to avoid a multitude of transition not relevant for the coming discussion. A polarization $P=0.9$ is chosen.

A. Differential conductance at zero magnetic field

Figures 10(a) and 10(b) show the stability diagrams for parallel and antiparallel lead magnetization, respectively, for the case of the $|a\rangle$ ground state. The two transition lines h and e were emphasized by a dashed line because these lines are so weak that it was not possible to resolve them together with the other stronger lines. The most obvious difference between the parallel and the antiparallel setup is the weakness of all transition lines beyond the triplet occupation (line b) for antiparallel lead magnetization. Moreover an NDC line, (line b), not present in the parallel magnetization case, is observed.

In order to explain the line positions in Figs. 10(a) and 10(b) we provide a schematic in Fig. 11 which is based on a bias trace at the particular gate voltage which aligns the ground states (white vertical lines in Fig. 10). The different arrows stand for new transport channels that open at certain

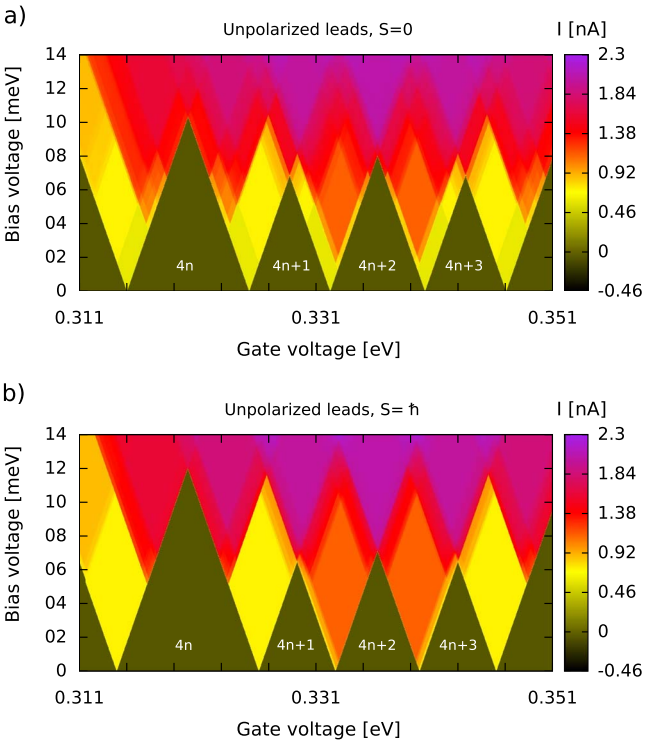

FIG. 9. (Color online) Current versus gate and bias voltages for unpolarized leads. In total 176 states have been included, which corresponds to all states with at most one bosonic excitation. For $4n+2$ filling this amounts to 32 different states. (a) Band mismatch $\epsilon_\Delta=0.3$ ϵ_0 corresponding to an $S=0$ ground state for the $4n+2$ filling. (b) Band mismatch $\epsilon_\Delta=0$ corresponding to an $S=\hbar$ ground state at filling $4n+2$. In both cases a four-electron periodicity of the Coulomb diamonds is observed.

bias voltages. The channels open in the order of a to e for transitions from $4n+1 \rightarrow 4n+2$ (dashed arrows) and f to h for transitions from $4n+2 \rightarrow 4n+1$ (solid arrows). Sometimes opening of a new channel also opens other channels that have been blocked before and one does not see distinct lines for these transitions. Figure 11 relates the concerned transitions to the required bias voltages. Moreover, the line g stands for transitions between the triplet and the $|\cdot, \sigma\rangle$ states, i.e., it is a transition between excited states.

To explain the NDC in Fig. 10(b) which follows upon line b in the range between lines f and line g, we observe that—in correspondence of the b line—below the resonance only the transitions from $|\sigma, \cdot\rangle$ to the $|a\rangle$ state is possible. Above resonance also the triplet $|t\rangle$ is accessible. For the case of antiparallel polarization, both provide only weak transport channels: below the resonance transport is mostly mediated by ↑ electrons (see also sketch of Fig. 5) which are minority electrons for the source contact; above resonance, after some tunneling processes the system will always end up in the $|t_{-1}\rangle$ state which is a trapping state. Just at the exact resonance, the thermal energy allows electrons to tunnel forth and back, i.e., a ↓ electron has the possibility to tunnel back into the source contact and transport is slightly enhanced. Once the bias voltage exceeds the exact resonance the trapping state $|t_{-1}\rangle$ gets occupied for long times and the current diminishes again.

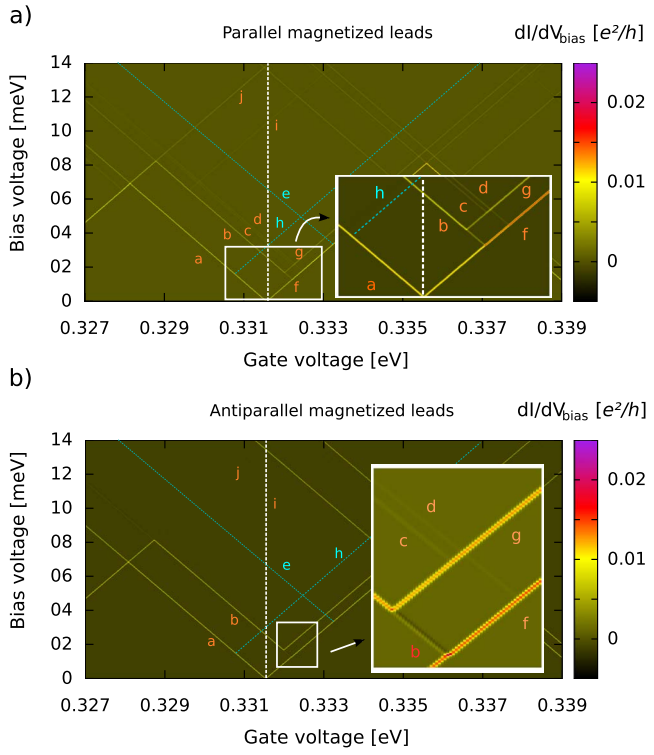

FIG. 10. (Color online) Differential conductance for transitions between $4n+1 \leftrightarrow 4n+2$ filling in the $|a\rangle$ ground state. The polarization has been chosen to be $P=0.9$. The four lowest lying states for $4n+1$ and the six ones for $4n+2$ filling were included. The vertical white line is the bias trace we follow to explain the distinct transition lines in Fig. 11. (a) The leads are magnetized in parallel. (b) Antiparallel magnetized leads. We observe a different intensity of the excitation lines between parallel and antiparallel magnetization. In particular a pronounced negative differential conductance (NDC) occurs in correspondence of the transition between $|\sigma,\cdot\rangle$ and the triplet (line b).

The fact that the $|\downarrow,\cdot\rangle \leftrightarrow |t_{-1}\rangle$ transition serves as the major transport channel once it has been opened is also the reason why all transition lines above line b are so weak.

In Figs. 12(a) and 12(b) the stability diagrams for the $S=\hbar$ triplet ground state are shown. They look a lot simpler

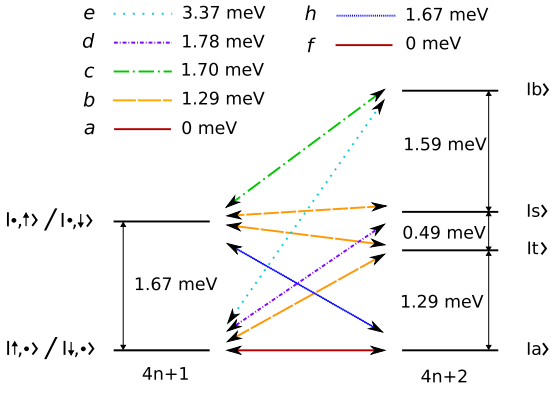

FIG. 11. (Color online) Schematic for the possible transitions occurring by sweeping the bias voltage at the gate voltage that aligns the $|\sigma,\cdot\rangle$ and the $|a\rangle$ states (white dashed line in Fig. 10).

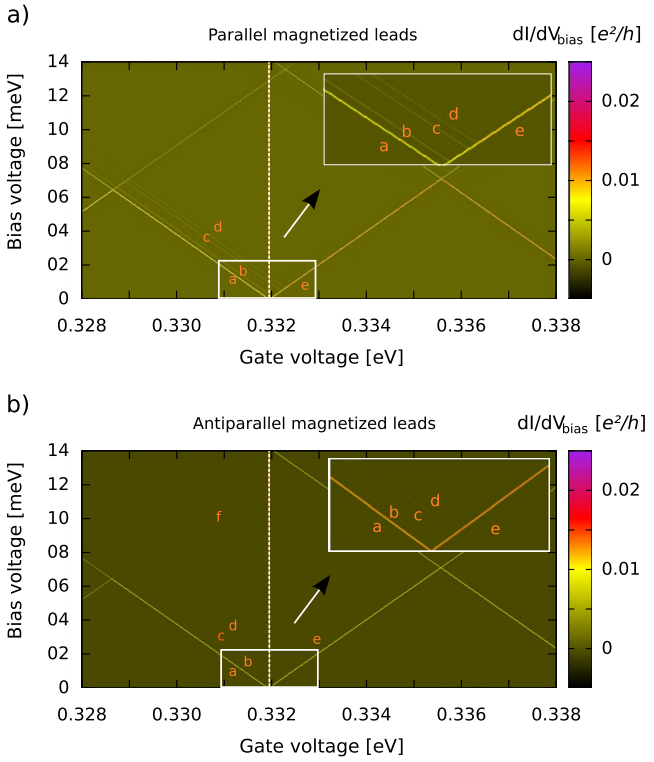

FIG. 12. (Color online) Differential conductance for transitions between $4n+1 \leftrightarrow 4n+2$ filling in the triplet ground state. The polarization has been chosen to be $P=0.9$. The four lowest lying states were included for $4n+1$ and the six lowest ones for $4n+2$. (a) Leads parallel magnetized. (b) Leads polarized antiparallel. From the stability diagrams it is possible to directly extract the exchange parameters u^+ and J since the bias voltage $V_b/2=u^+$ is needed to open transition line b and $V_b/2=J$ to open line c.

than the ones in Fig. 10 due to the absence of a band mismatch, causing a degeneracy of all four $4n+1$ filling ground states. Line a is the ground state to ground-state transition. Lines b to d indicate transitions from the $4n+1$ ground states to $|a\rangle$, $|s\rangle$, and $|b\rangle$, respectively. They come in the expected order, at an applied voltage $V_b/2$ equal to u^+, J, and $J+u^+$, as it is shown in Table I. Line e stands for the transition from the triplet to one of the $4n+1$ ground states.

For the antiparallel setup, Fig. 12(b), we may see the same effect as we have observed in Fig. 10(b), i.e., all lines beyond the transition to the triplet decrease in intensity. Since the triplet is the ground state, this means all excitation lines are weak and may not be resolved in the figure.

B. Differential conductance in parallel magnetic field

Here we present results for an applied magnetic field of strength $E_z=0.1$ meV, Fig. 13. The leads are parallel magnetized and a polarization of $P=0.6$ has been applied. The magnetic field removes the spin degeneracy of the triplet as well as of the $4n+1$ filled states; the resulting Zeeman split transitions are clearly seen in Fig. 13(a) and are less well resolved in Fig. 13(b).

Explicitly, for the $|a\rangle$ ground state, line b from Fig. 10 splits into lines b and c in Fig. 13. We notice that line c

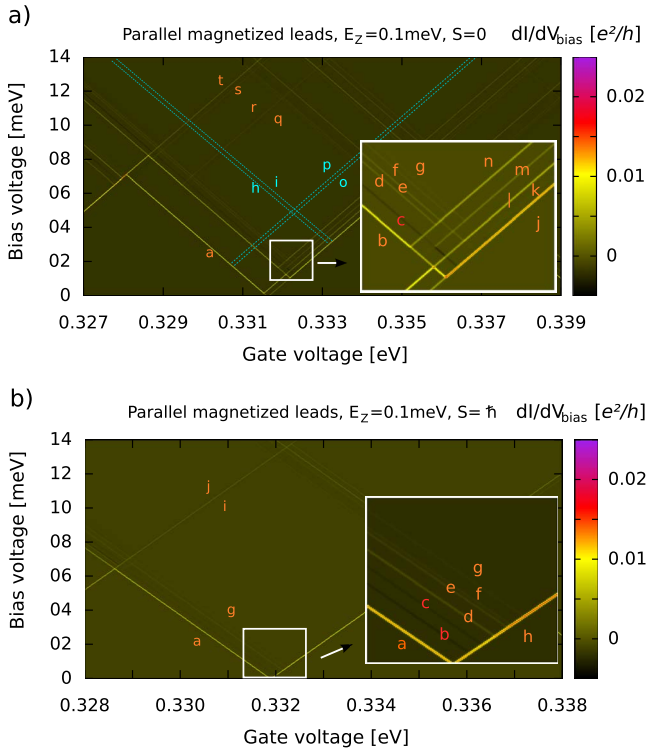

FIG. 13. (Color online) Differential conductance for transitions between $4n+1 \leftrightarrow 4n+2$ filling with an applied magnetic field of $E_z=0.1$ meV. A parallel lead magnetization was assumed with the polarization $P=0.6$. (a) $|a\rangle$ ground state. Soon after line c an NDC effect is observed due to the occupation of the $|t_{-1}\rangle$ trapping state. (b) Triplet ground state. After lines b and c NDC occurs due to an increased population of the $|t_{-1}\rangle$ state.

shows an NDC effect due to the opening of the channel $|\downarrow,\cdot\rangle \rightarrow |t_{-1}\rangle$: though this transition, as mediated by minority $\downarrow$ electrons, is rare, once it happens the system is trapped in the $|t_{-1}\rangle$ state for a long time due to the parallel polarization of the leads. For transitions from $4n+2$ to $4n+1$ line k is a new line that was Coulomb blocked in Fig. 10. It denotes the transition $|s\rangle \rightarrow |\cdot,\downarrow\rangle$ and ends in line e since the $|s\rangle$ state must be populated. Also, we notice the absence of the $|s\rangle \rightarrow |\uparrow,\cdot\rangle$ line since it is Coulomb blocked by the ground state to ground state transition (line j).

For the $S=\hbar$ triplet ground state, Fig. 13(b), we observe that line b and line c show NDC effects. Line b represents transitions from $|\cdot,\uparrow\rangle \rightarrow |t_0\rangle$ or $|\uparrow,\cdot\rangle \rightarrow |t_0\rangle$, which is not a trapping state. However, the applied bias voltage is sufficient to also populate the $|\cdot,\downarrow\rangle$ and $|\downarrow,\cdot\rangle$ states from $|t_0\rangle$ and subsequently from $|\cdot,\downarrow\rangle$ and $|\downarrow,\cdot\rangle$ the trapping state $|t_{-1}\rangle$. This process is also visualized in Fig. 14. In the very same way it is possible to get trapped in the $|t_{-1}\rangle$ state via the $|a\rangle$ state indicated by line c.

C. Magnetic field sweep

In a seminal experiment Moriyama *et al.*[8] demonstrated a transition from a $S=0$ ground state to a $S_z=\hbar$ ground state upon magnetic field sweep in a SWNT quantum dot. In this section we have computed the differential conductance in a

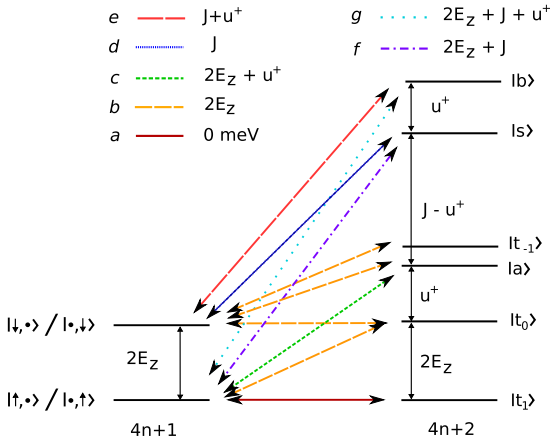

FIG. 14. (Color online) Schematic of the possible transitions if the $|\cdot,\uparrow\rangle$ and $|\uparrow,\cdot\rangle$ states are aligned to the $|t_1\rangle$ state by the gate voltage at finite magnetic field and in the triplet ground state. It provides the explanation for the transitions lines observed in the inset of Fig. 13(b).

gate voltage and magnetic field plot both for unpolarized, as in Ref. 8, and parallel polarized leads with $P=0.9$.

We start from the $|a\rangle$ ground state at $B=0$ with a band mismatch of $0.24\epsilon_0$ (smaller than we previously used). This choice yields a change of ground state from $|a\rangle$ to the triplet at a magnetic field $\simeq 6$ T as measured experimentally.[8] To observe well visible patterns, we increased the temperature by a factor of 10 compared to Table II.

The result of our calculation is presented in Fig. 15(a). At a gate voltage of approximately 0.322 and 0.323 meV we have two "V"-shaped transition patterns (a and b) each of width $2E_z=2\mu_B B$. The separation between a and b at zero field is the band mismatch ϵ_Δ. Interestingly, for polarized leads, the branches belonging to transitions involving $(|\downarrow,\cdot\rangle,|\cdot,\downarrow\rangle)$, corresponding to the positive slope of the "V," are NDC lines, Fig. 15(b). The reason is the same as addressed already in Sec. V B, once the $\downarrow$ channel becomes available, there is some chance that from time to time a minority charge carrier ($\downarrow$ electron) enters from the source. As the drain is polarized in parallel to the source, it will take quite a while until this electron can leave the SWNT again, such that transport gets hindered. At the gate voltage of approximately 0.328 meV, one enters the $N_c=4n+1$ Coulomb diamond (line c) and transport gets completely suppressed. The dot is in the ground state $|\uparrow,\cdot\rangle$ at $B \neq 0$. At $V_g \simeq 0.329$ meV transport from $N_c=4n+1$ to the $|a\rangle$ state is enabled (line d).

The next transitions (patterns e, f, and g) we observe are again split by $2E_z$ and therefore shaped like a "V." In all cases, the positively sloped branches are now again of NDC nature for a parallel lead polarization. The first "V" belongs to the triplet (pattern e) and is of stronger intensity than the following two patterns. The transitions $|\uparrow,\cdot\rangle \leftrightarrow |t_1\rangle$ and $|\downarrow,\cdot\rangle \leftrightarrow |t_0\rangle$ contribute to the negative sloped part, while $|\uparrow,\cdot\rangle \leftrightarrow |t_0\rangle$ and $|\downarrow,\cdot\rangle \leftrightarrow |t_{-1}\rangle$ are responsible for the positive shaped line. The crossing of the e and d lines occurring at $B \cong 6$ T, point P, indicates *the change in the ground state from* $|a\rangle$ to the state $|t_1\rangle$.

From the triplet pattern e the additional gate voltage equal to the exchange energy J is needed to arrive at the last two

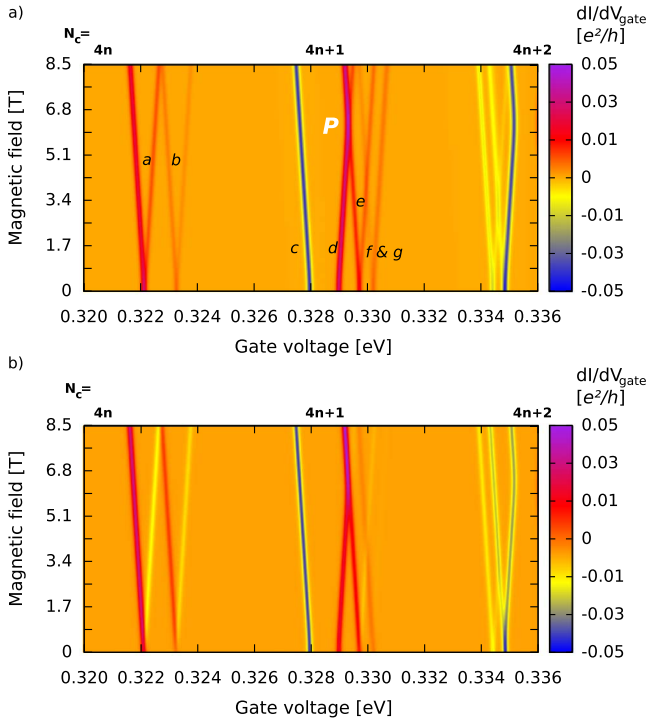

FIG. 15. (Color online) (a) Differential conductance dI/dV_g for a B-field sweep in the $|a\rangle$ ground state case. The applied bias voltage was fixed at 5.8 meV. Red lines indicate transitions that become possible at a certain gate voltage and blue lines show a transition that drops out of the transport window. The "V"-shaped patterns a and b represent transitions from $N_c=4n$ to $|\sigma,\cdot\rangle$ and $|\cdot,\sigma\rangle$, respectively. Each of the patterns is split by $2E_z$ denoting $\uparrow$ electrons and $\downarrow$ electrons tunneling in. At line c we enter the $N_c=4n+1$ Coulomb diamond and transport gets suppressed. Line d stands for the ground state to ground state transition from $|\uparrow,\cdot\rangle$ to the $|a\rangle$ state. The "V"-shaped pattern e is due to the transition $N_c=4n+1$ to the triplet whereas f and g denote transitions to the $|s\rangle$ singlet and the $|b\rangle$ state, respectively. At the point P the ground state changes from the $|a\rangle$ state to the $|t_1\rangle$ triplet. (b) Ferromagnetic leads, polarized in parallel with $P=0.9$, are assumed. This changes the intensity of the transitions, while their positions are preserved. Moreover, transitions to excited states involving spin-down electrons are disfavored channels and hence converted from positive to negative differential conductance lines.

"V"-shaped patterns f and g. Compared to the lines for the triplet transition they are quite close to each other and of less intensity. These lines belong to a transition from both the $|\downarrow,\cdot\rangle$ and the $|\uparrow,\cdot\rangle$ states to the $|s\rangle$ singlet (pattern f) and the $|b\rangle$ state (pattern g). Finally, the lines on the right edges of the plots are mirror images and belong to backward transitions from $N_c=4n+2$ to $N_c=4n+1$; for this reason they mark a decrease in current for both polarized and unpolarized leads.

VI. CONCLUSIONS

In summary, we have calculated spin-dependent transport through fully interacting SWNTs in both the linear and the nonlinear regime, with and without an applied magnetic field.

Peculiar of metallic SWNTs of small diameter is the possibility, due to exchange interactions, to find the system at $4n+2$ filling either in a ground state of total spin $S=0$ or $S=\hbar$. Which of the two ground states occurs in a real nanotube depends on the relation between the exchange energy and the orbital band mismatch. Thus, with focus on transitions involving $4n+1\leftrightarrow 4n+2$ filling, we investigated both situations and demonstrated pronounced differences in the current-voltage characteristics depending on the considered ground state.

For example in the linear regime the conductance for parallel lead magnetization and finite magnetic field increases by raising the polarization for the case of a triplet ground state but it decreases for the $S=0$ ground state. This is due to the fact that for the triplet ground state transport is dominated by a channel involving the triplet state $|t_1\rangle$ (with both spins $\uparrow$); for the $S=0$ case transport to be mediated by the majority electrons requires to make use of the $4n+1$ lowest excited state $|\downarrow,\cdot\rangle$ (and hence less favorable), Zeeman split from the ground state.

In the nonlinear regime we presented stability diagrams with parallel and antiparallel lead magnetization for both ground sates. In the antiparallel case it was possible to observe a negative differential conductance effect for the $S=0$ ground state, following immediately upon a conductance enhancement at the opening of a trapping channel to the excited triplet state $|t_{-1}\rangle$. Directly at that resonance, electrons can, just by thermal activation, tunnel back *and* fourth, such that trapping in the $|t_{-1}\rangle$ state cannot yet act, leading to an intermediate conductance increase. Away from resonance, the blocking effect fully occurs, resulting in the NDC. By adding an external magnetic field in the parallel setup we found NDC effects for both ground states caused by spin blocking mediated by $\downarrow$ channels, involving in particular the triplet state $|t_{-1}\rangle$.

Finally, we also presented results for the differential conductance in a gate voltage and magnetic field map at finite bias. These magnetic field sweeps immediately allow to recognize the nature of the $4n+2$-filling ground state at zero field, as well as to tune the nature of the ground state from $S=0$ to $S_z=\hbar$ upon variation in the field amplitude. Our results for unpolarized leads are in *quantitative* agreement with experiments on a small-diameter SWNT by Moryama *et al.*[8] Importantly the sweep at zero field also allows to immediately read off the values of the short-range interactions J and u^+. Specifically, J is the singlet-triplet exchange splitting and u^+ characterizes at zero orbital mismatch the energy difference between two of the low energy states of total spin $S=0$. In the presence of polarized leads the magnetic field sweep also reveals lines of NDC due to the trapping nature of all $\downarrow$ channels.

The predictions of our theory are in quantitative agreement with experimental results obtained so far for unpolarized leads.[8–10] Due to recent achievements on spin-polarized transport in SWNTs,[12–14] our predictions on spin-dependent transport are within the reach of present experiments.

ACKNOWLEDGMENTS

We acknowledge support by the DFG under the funding programs SFB 689 and GRK 638.

[1] S. Iijima and T. Ichihashi, Nature (London) **363**, 603 (1993).
[2] R. Saito, G. Dresselhaus, and M. Dresselhaus, *Physical Properties of Carbon Nanotubes* (Imperial College Press, London, 1998).
[3] A. Loiseau, P. Launois, P. Petit, S. Roche, and J.-P. Salvetat, *Understanding Carbon Nanotubes, Lecture Notes in Physics* (Springer, Berlin, 2006).
[4] R. Egger and A. O. Gogolin, Phys. Rev. Lett. **79**, 5082 (1997).
[5] A. A. Odintsov and H. Yoshioka, Phys. Rev. B **59**, R10457 (1999).
[6] Y. Oreg, K. Byczuk, and B. I. Halperin, Phys. Rev. Lett. **85**, 365 (2000).
[7] L. Mayrhofer and M. Grifoni, Eur. Phys. J. B **63**, 43 (2008).
[8] S. Moriyama, T. Fuse, M. Suzuki, Y. Aoyagi, and K. Ishibashi, Phys. Rev. Lett. **94**, 186806 (2005).
[9] S. Sapmaz, P. Jarillo-Herrero, J. Kong, C. Dekker, L. P. Kouwenhoven, and H. S. J. van der Zant, Phys. Rev. B **71**, 153402 (2005).
[10] W. Liang, M. Bockrath, and H. Park, Phys. Rev. Lett. **88**, 126801 (2002).
[11] A. Cottet, T. Kontos, S. Sahoo, H. T. Man, M.-S. Choi, W. Belzig, C. Bruder, A. F. Morpurgo, and C. Schönenberger, Semicond. Sci. Technol. **21**, S78 (2006).
[12] S. Sahoo, T. Kontos, J. Furer, C. Hoffmann, M. Gräber, A. Cottet, and C. Schönenberger, Nat. Phys. **1**, 99 (2005).
[13] H. T. Man, I. J. W. Wever, and A. F. Morpurgo, Phys. Rev. B **73**, 241401(R) (2006).
[14] J. R. Hauptmann, J. Paaske, and P. E. Lindelof, Nat. Phys. **4**, 373 (2008).
[15] L. Balents and R. Egger, Phys. Rev. Lett. **85**, 3464 (2000).
[16] C. S. Peça, L. Balents, and K. J. Wiese, Phys. Rev. B **68**, 205423 (2003).
[17] S. Koller, L. Mayrhofer, and M. Grifoni, New J. Phys. **9**, 348 (2007).
[18] I. Weymann, J. Barnas, and S. Krompiewski, Phys. Rev. B **76**, 155408 (2007).
[19] I. Weymann, J. Barnas, and S. Krompiewski, Phys. Rev. B **78**, 035422 (2008).
[20] W. Barford, *Electronic and Optical Properties of Conjugated Polymers* (Clarendon Press, Oxford, 2005).
[21] P. Fulde, *Electron Correlations in Molecules and Solids* (Springer, Berlin, New York, 1995).
[22] L. Mayrhofer and M. Grifoni, Eur. Phys. J. B **56**, 107 (2007).
[23] J. von Delft and H. Schoeller, Ann. Phys. **7**, 225 (1998).
[24] H. Yoshioka and A. A. Odintsov, Phys. Rev. Lett. **82**, 374 (1999).
[25] V. V. Deshpande, B. Chandra, R. Caldwell, D. S. Novikov, J. Hone, M. Bockrath, Science **323**, 106 (2009).